CHAPTER-6

EFFECT OF SOLUTION TREATMENT AND AGEING ON Al-Mg_2Si FUNCTIONALLY GRADED COMPOSITES

6.1 Introduction

In Al-Mg_2Si in-situ composites the as-cast tensile properties are not appreciable due to coarse Mg_2Si particles and silicon morphology in eutectic formed during solidification. This restricts the wide spread applications of this composites. Apart from chemical modifications with several alloying additions, heat treatment like solution treatment and ageing are effective means to refine the structure as well as to form additional extra-fine precipitates during ageing. The heat treatment provides several microstructural changes which include homogenization, better distribution of alloying elements, and dissolution of soluble phases with Si and Mg and spheroidization of eutectic particles, obviously results in a remarkable improvement in mechanical properties [103]. The dissolution of Mg_2Si particles is attributed to high rate of diffusion of Mg in the Al matrix at the pretty high solution treatment temperature. The objective of the solution treatment is not to dissolve totally the primary Mg_2Si particles formed during solidification but to refine the coarse particles by surface diffusion. In view of this, the present chapter deals with the effects of solution heat treatment and subsequent ageing treatment on the microstructure and consequent mechanical properties of A356-Mg_2Si in-situ FG-composites.

6.2 Effect of solution treatment and ageing on microstructure

The base alloy and the composites were solution treated at 495°C for 7 h, hot water quenched (90^0C) and subsequently artificially aged at 160°C for 10 h in steps of 1h. The

solution treated and artificially aged A356 base alloy microstructures at different zones are shown in Fig.6.1. For comparison the as-cast microstructures are shown as well. The eutectic Si is showing a remarkable change in the morphology from coarse acicular particles to fragmented more or less spheroidized refined particles. The spheroidization of Si particles has been reported to take place in two stages [104]:

- Fragmentation or dissolution of the eutectic Si-branches
- Spheroidization of separated branches.

In the first stage of fragmentation, Si particles undergo necking and separate into segments. The average particle size decreases due to separation and subsequently fragmented segments are converted to spheroids. From the microstructures, it is evident that, a large number of Si particles are more or less spheroidized and still a considerable number of particles are of rod-like shape. The α-Al dendrites are refined and Fe-intermetallics are rarely seen in the microstructure.

Optical microstructures of solution treated and aged FG-composites are shown in Figs.6.2 to 6.5. Similar to the base A356 alloy the eutectic Mg_2Si particles are more or less spheroidized. In regard to primary Mg_2Si particles a considerable refinement could be observed. Beside the refinement there is a change in the shape of the Mg_2Si particles, the sharp corners of Mg_2Si octahedron in the as –cast structure are rounded at the edges during solution treatment. In coarse of solution treatment diffusion of Mg and Si in to the matrix proceeds preferentially from the positions with large curvature and convexity to the flat interface having lower atomic concentration [105,106]. With 10 wt.% Mg, a large number

of dot-like eutectic is observed and primary blocky Mg_2Si are almost absent in the outer zone.

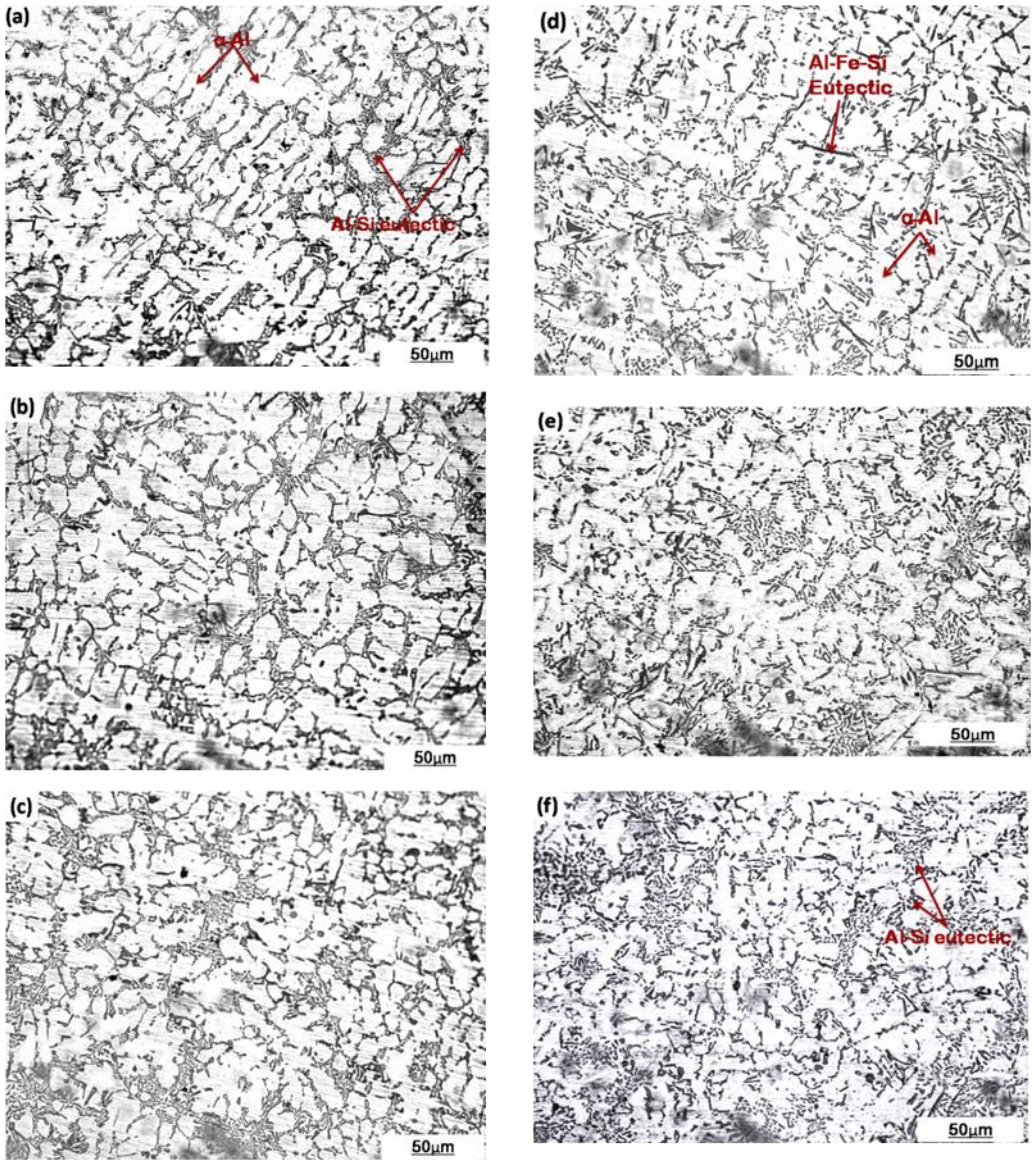

Fig.6.1. Microstructures of A356 alloys (a), (b), (c) solution treated conditions and (d), (e),(f) solution treated at 495°C and after ageing for 7 h time at inner, middle & outer layers respectively.

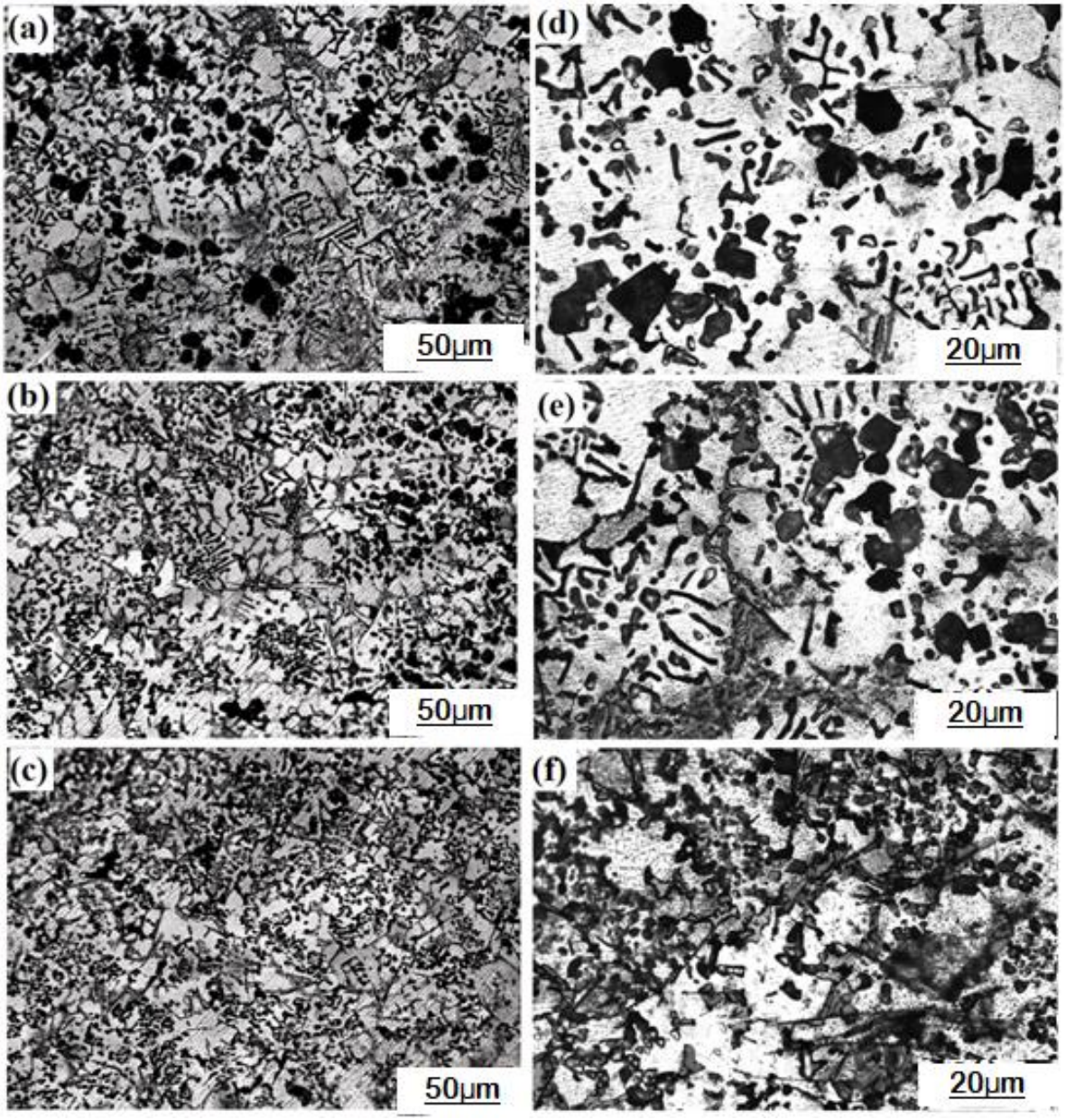

Fig.6.2. Optical microstructures of A356+2.5Mg FG composites at inner, middle & outer layers respectively; (a),(b),(c) are in solution treated conditions and (d),(e),(f) are after ageing treatment.

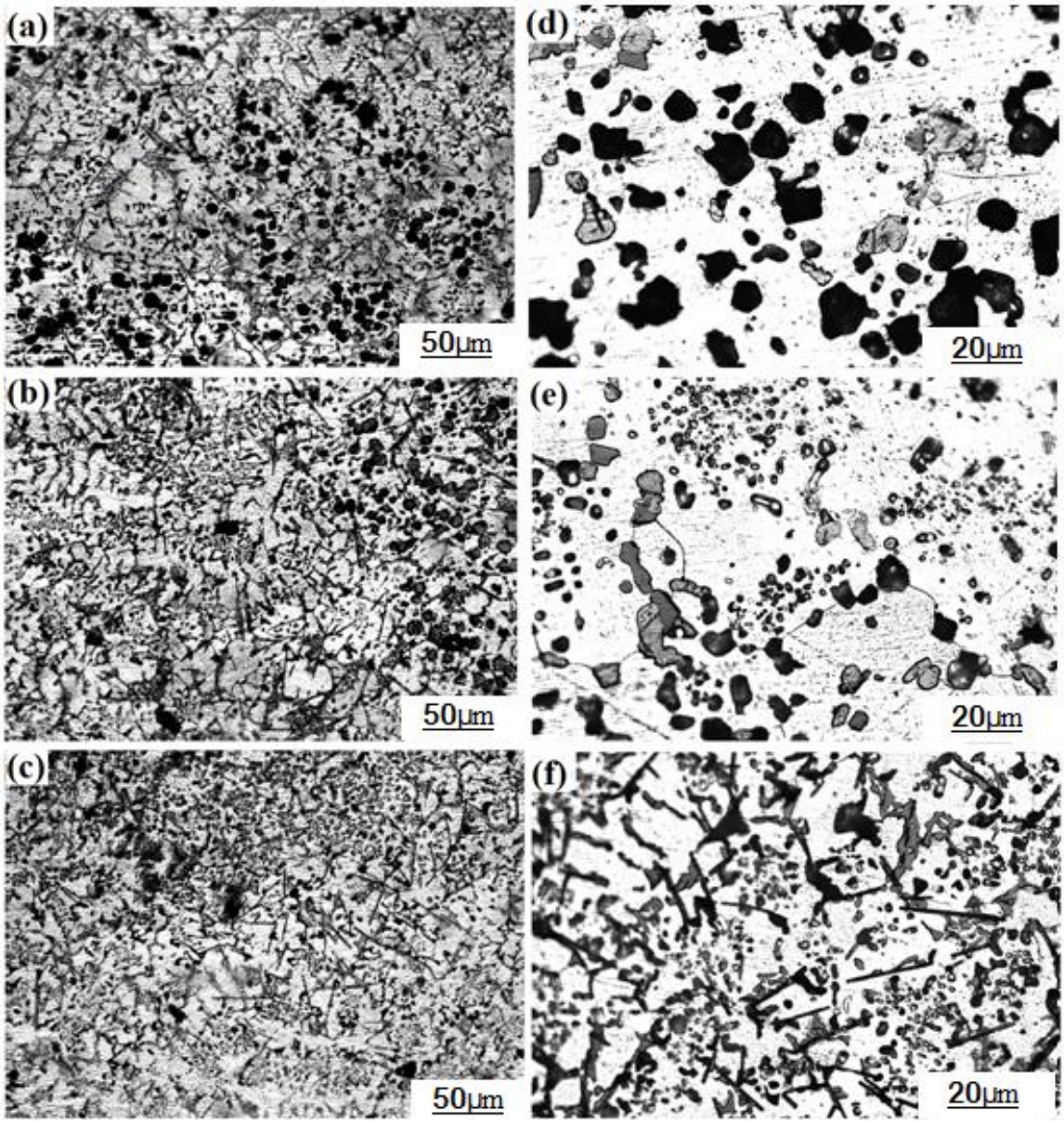

Fig.6.3 Optical microstructures of A356+5Mg FG composites at inner, middle & outer layers respectively; (a),(b),(c) are in solution treated conditions and (d),(e),(f) are after ageing treatment.

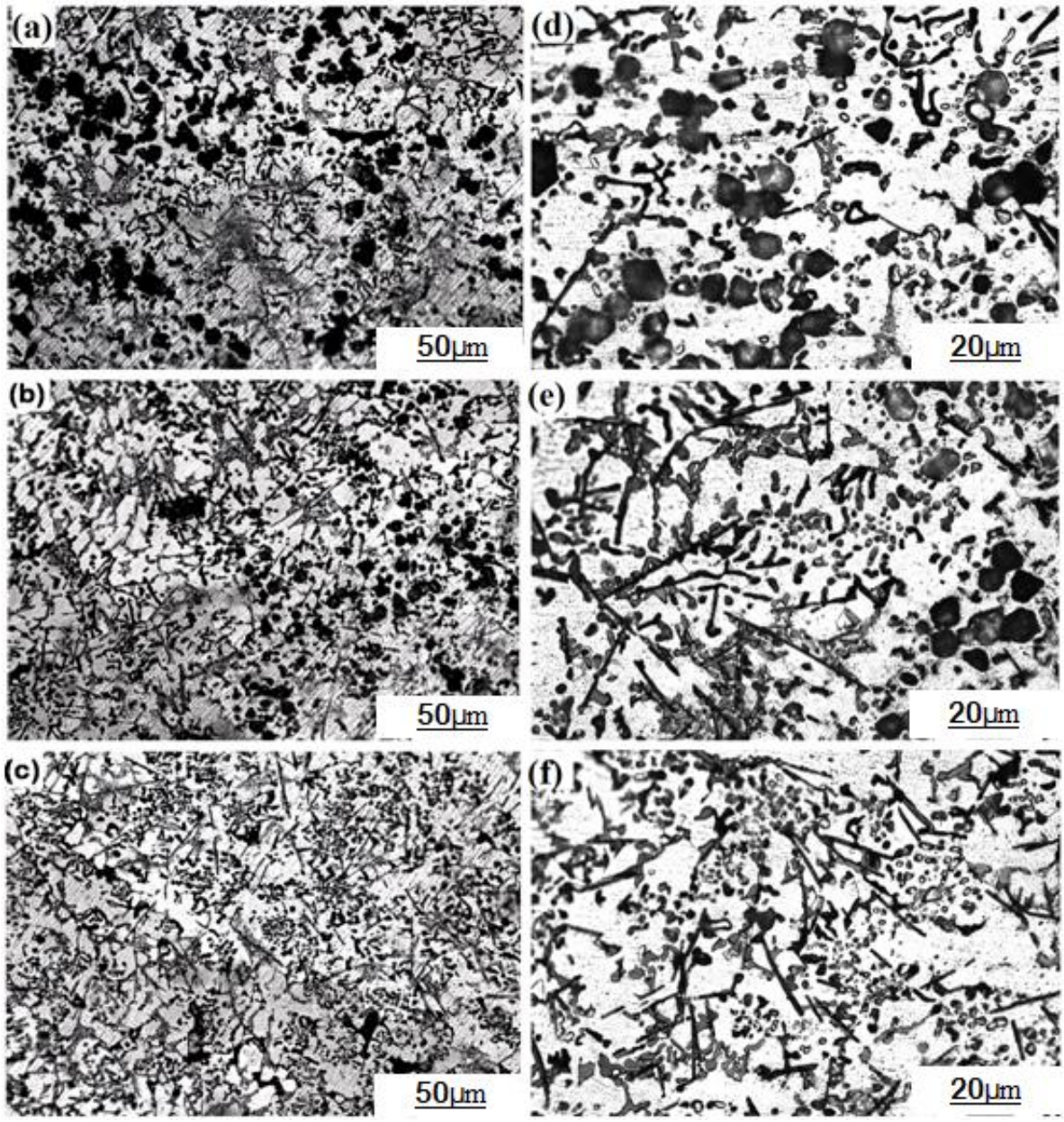

Fig.6.4 Optical microstructures of A356+7.5Mg FG composites at inner, middle & outer layers respectively; (a),(b),(c) are in solution treated conditions and (d),(e),(f) are after ageing treatment.

The effects of T6 heat treatment on the microstructure of FG-composites were examined further under SEM and are illustrated in Figure 6.6 & 6.7. It can be seen from the Fig.6.6 (a) as-cast condition the eutectic Si phase is present in the form of coarse acicular particles.

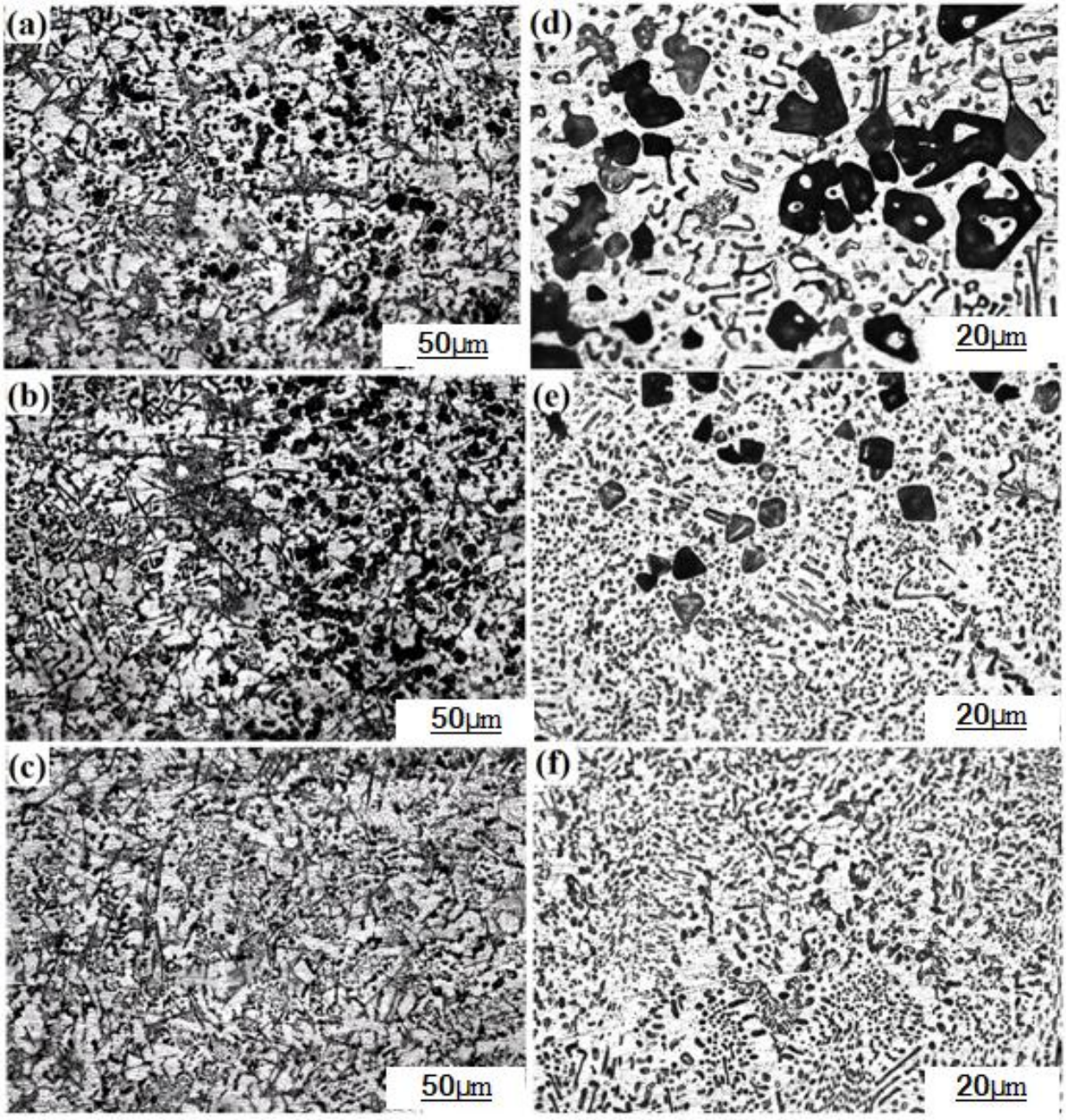

Fig.6.5 Optical microstructures of A356+10Mg FG composites at inner, middle & outer layers respectively; (a),(b),(c) are in solution treated conditions and (d),(e),(f) are after ageing treatment.

After solution treatment and ageing, spheroidization of eutectic Si are prominent in the structures which results in predominantly very fine dot-like eutectic structures. During ageing several micro- and nano- sized precipitates are formed from the supersaturated solid solution. Beside these freshly formed precipitates during ageing, some intermetallics such

as flaky Fe- intermetallic and some $CuAl_2$ of script morphology which were formed during solidification are also discernible [107]. However, the size of Fe-intermetallics are reduced remarkably in course of solution treatment.

The sequence of precipitation from supersaturated solid solution (ssss) in Al-Si-Mg alloys has been reported to be described as follows [108]:

- Precipitation of GP zones, (needles about 10 nm long);
- Intermediate phase β″-Mg_2Si, (homogeneous precipitation);
- Intermetallic phase β′-Mg_2Si, (heterogeneous precipitation);
- Equilibrium phase β-Mg_2Si, FCC structure (a= 0.639), rod or plate-shaped.

High concentration of quenched vacancies increases the clustering of solute and this will reduce matrix supersaturation with solute. Eventually these clusters act as nucleation sites for formation of β' precipitates during artificial ageing. The nuclii will not be stable if these are below the critical nucleus size. Moreover, a lower solute supersaturation will cause reduction in precipitation kinetics. Hence, solute concentration is increased by dissolution of unstable clusters and larger stable clusters grow to GP zones. These GP zones are subsequently acting as nucleation sites for β' precipitates.

When Cu is present in small percentage (in the present study is about 0.6%) in the base alloy, the precipitation sequence more complex as the Q'' ($Al_2Cu_2Mg_8Si_6$) phase and the θ' ($CuAl_2$) phase may also additionally form. Cu influences to increase the fraction of the β'' phase formed. However, it can also form the Q'' phase, having lower strength in comparison to the β'' phase. The β'' phase is therefore preferred, rather than the Q'' phase [108]. Sequences reported are not consensus; two possible sequences are:

i) SSSS →solute clusters →GP → ß", L,S,C,QP,QC →ß', Q'→Q(ß)

ii) SSSS →solute clusters →GP →ß" →ß', Q" →Q', θ', Si →Q, θ, Si

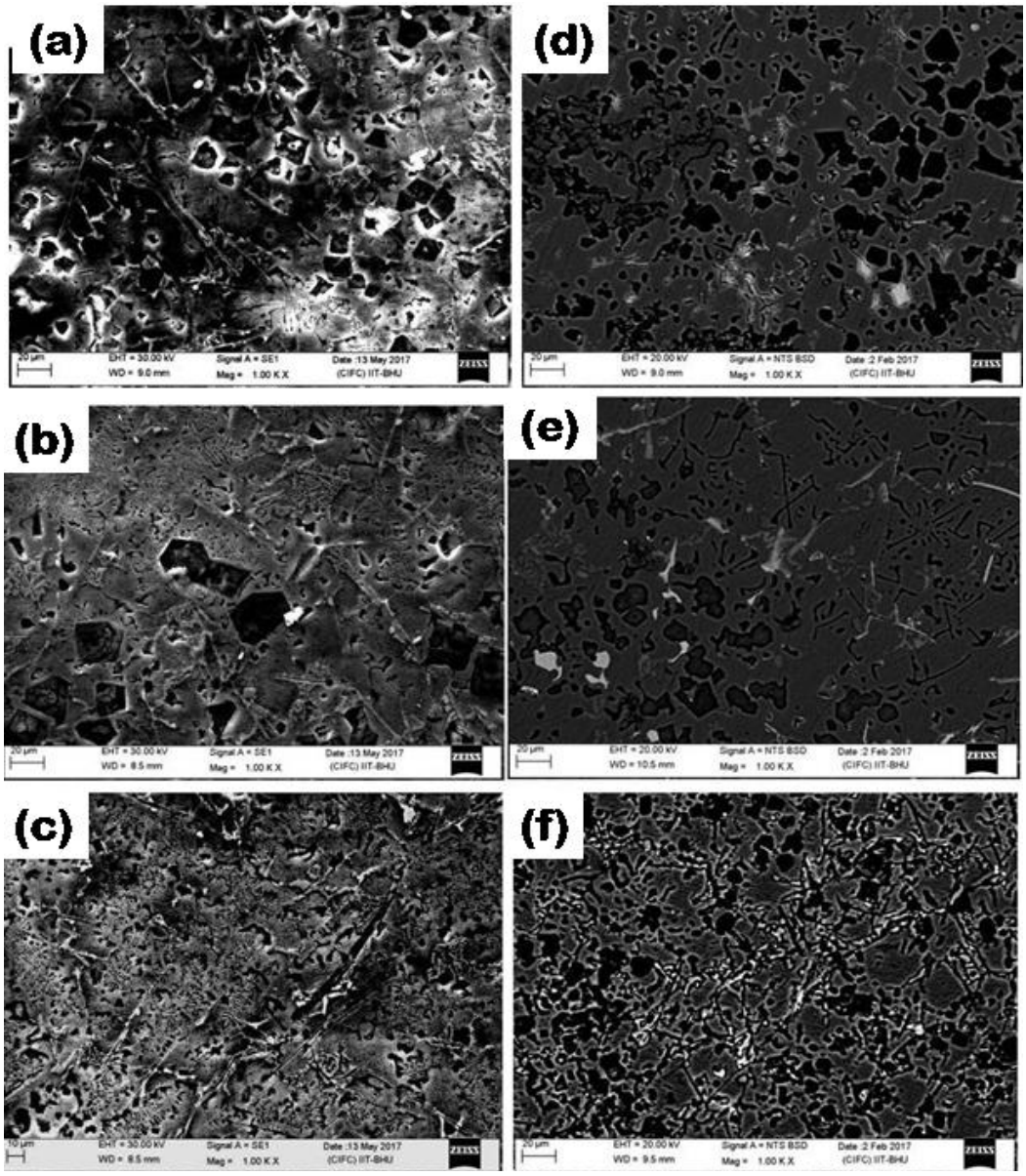

Fig.6.6 SEM images of A356+5Mg FGMs (a), (b), (c) as cast conditions and (d), (e), (f) after aged treated at 160°C for 7 hours at inner, middle & outer layers respectively.

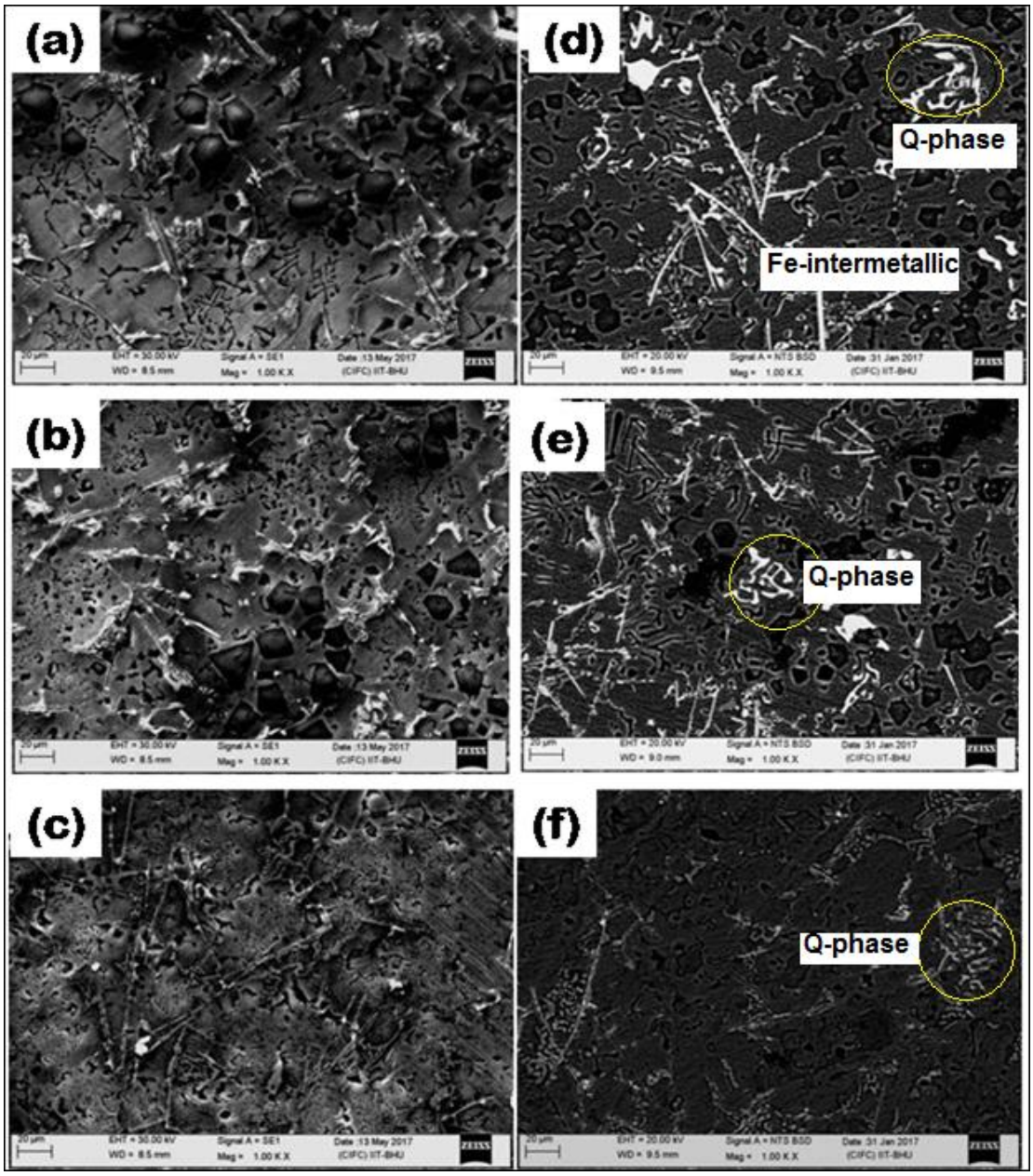

Fig.6.7 SEM images of A356+10Mg FGMs (a), (b), (c) as cast conditions and (d), (e), (f) after aged treated at 160°C for 7 h at inner, middle & outer layers respectively.

The analysis of XRD pattern after heat treatment of base alloy and FG-composites as shown in Fig.8 reveals the phases namely α-Al, Mg_2Si, Al_2Cu and Si in the four composites fabricated and Al_2Cu,α-Al and Si in the base A356 alloy. This is in conformity with the fabricated alloy and FGM microstructure illustrated in Figs. 6.2 to 6.5. However,

Q-phases ($Al_2Cu_2Mg_8Si_{6)}$ and Al-Fe-Si intermetallics are not detected in XRD analysis probably due to their small percentage in the composites.

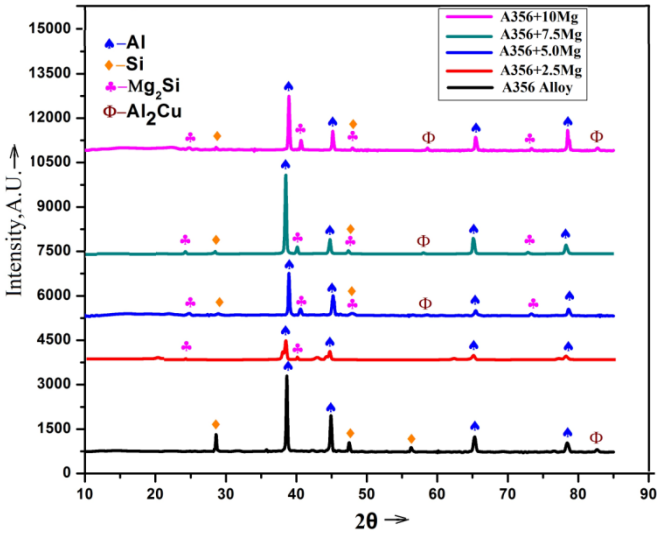

Fig.6.8 XRD Pattern of A356 alloy and FG-composites after heat treatment

6.3. Volume fraction and size distribution of primary Mg_2Si particles

As stated earlier, the main objective of the solution treatment and ageing treatment of FG composites is to refine the eutectic structure and change the morphology of primary Mg_2Si particles mainly segregated in the inner core regions of the cast tubes. The refinement of the primary Mg_2Si particles is not so prominent from the microstructures. The volume percent and respective size distributions have been analyzed by image analysis and are shown in Fig.6.9-10 with increasing wt.% of Mg in the composites. The analysis substantiates the microstructural observations. It could be further noticed that, as the wt.% Mg is increased the average size range of Mg_2Si particles are marginally reduced. The average size range is 21-25μm. This agrees the earlier findings on the size of the primary Mg_2Si [112].

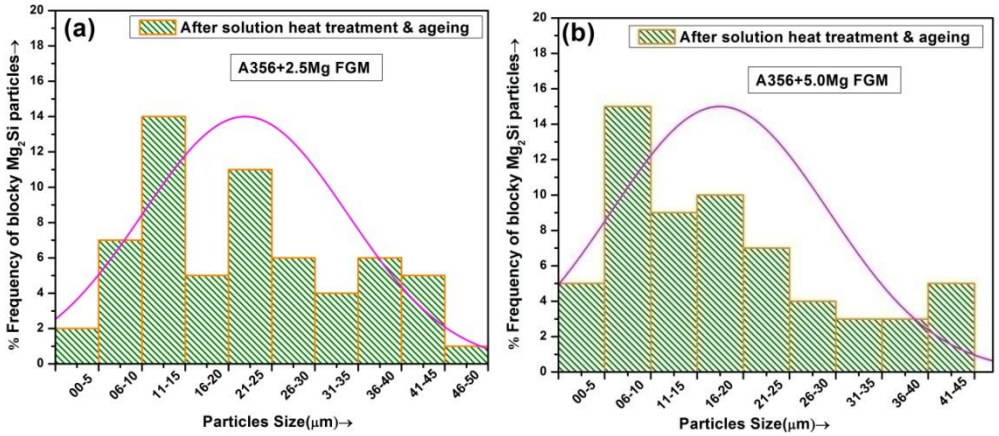

Fig. 6.9. Size distribution of Mg_2Si particles at inner zone of (a) A356+2.5Mg FG composite and (b) A356+5.0Mg FG composite after T6 treatment.

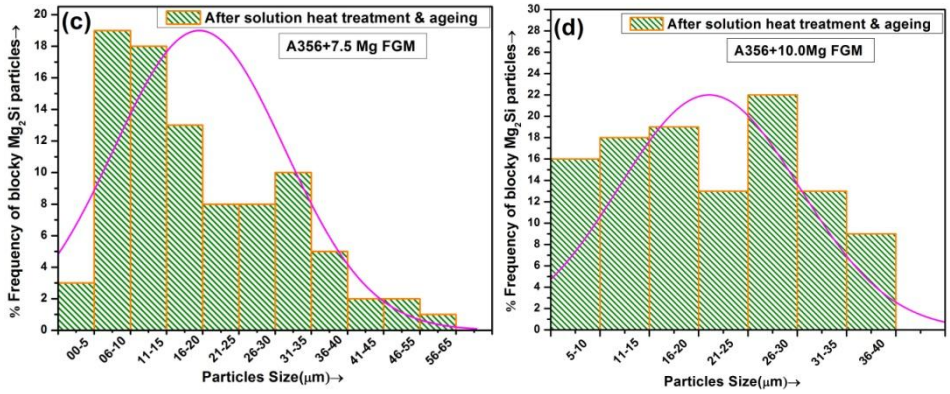

Fig. 6.10. Size distribution of Mg_2Si particles at inner zone of (c) A356+7.5Mg FG composite and (d) A356+10.0Mg FG composite after T6 treatment.

6.4. Transmission Electron Microscopy on aged samples

The bright field TEM micrographs of solution treated and aged samples related to ageing peaks and the corresponding selected area diffraction patterns (SADP) are shown in Figs. 6.11 and 6.12. The rod-shaped and disc-shaped precipitates are formed during the ageing treatment. The analysis of SADP reveals that, these are metastable β' and incoherent equilibrium β precipitates respectively. At peak aged samples in some locations the transition from β' to β has been occurred.

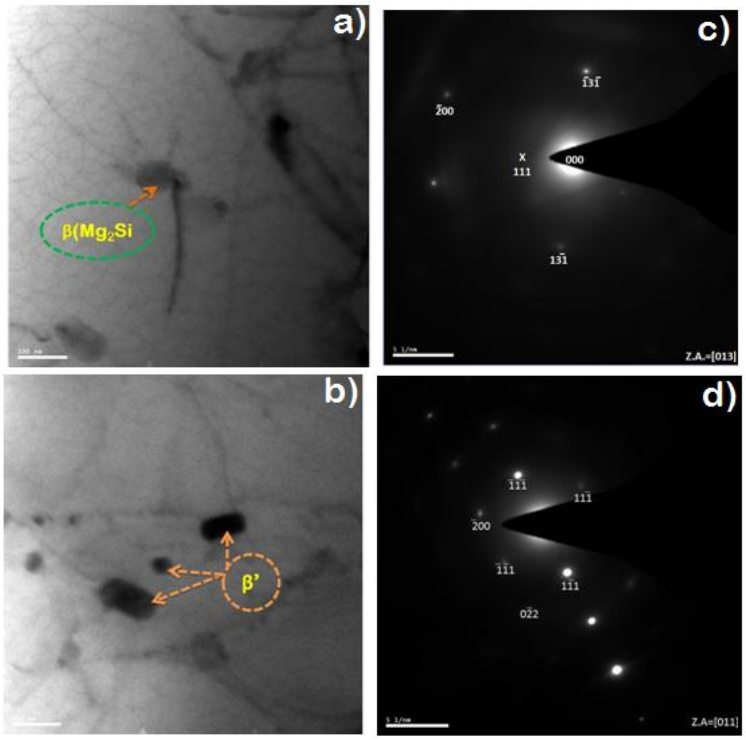

Fig. 6.11. TEM-BF micrographs show precipitated phases related to peak-aged condition and corresponding SADPs from Mg_2Si precipitates indicated by the arrows for (a) A356+2.5Mg and (b) A356+5.0Mg FG- composites respectively.

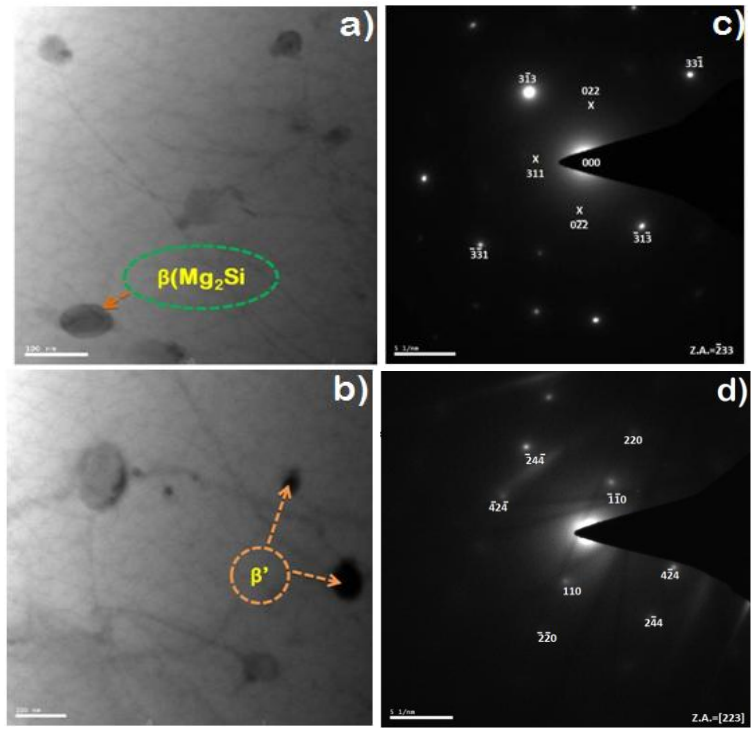

Fig. 6.12. TEM-BF micrographs show precipitated phases related to peak-aged condition and corresponding SADPs from Mg_2Si precipitates indicated by the arrows for (a) A356+7.5Mg and (b) A356+10Mg FG- composites respectively.

6.5. Effect on mechanical properties

6.5.1 Ageing effect on hardness

The Vickers Hardness profiles of different zones FG-composites such as inner, middle and outer zones are shown in Fig.6.13 of (a)A356 alloy, (b)A356+2.5Mg,(c) A356+5.0Mg, (d)A356+7.5Mg & (e)A356+10.0Mg FG-composites respectively. From the ageing curves it is evident that, two consecutive hardness peaks are revealed in the base alloy and three peaks in the composites are seen with the progress of ageing. The first peak hardness is attained at an approximate ageing time of 3-4 h while the second and third peaks have been attained at around 7h and 9h of ageing respectively. These multiple peaks could be attributed to the sequence of precipitation. In the initial stages of ageing the super saturated solid solution (ssss) forms a large number of GP zones and remains in a coherent state with the matrix. Consequently, the hardness increases and the first peak is appeared. As the ageing proceeds GP zones turn into ß". These ß" growing with the ageing time result in decrease in hardness. Further continuation of ageing ß" are converted to ß' and hardness again increases forming the second peak. Now, if Cu is present the second peak is not only due to ß' precipitates but also due to another metastable precipitate of Q". These Q'' precipitates can only be detected by HRTEM. The second peak is the highest peak among the three peaks indicating the effect of ß' and/or Q" phase strengthening is greatest. Q" is the precursor of Q'. As ageing continues Q" is converted to metastable Q' with some ß' and θ' as well. These three phases giving rise to third ageing peaks which are not so intense as second peaks. Ultimately, the equilibrium precipitates of Q, ß and θ are formed with decrease in age hardness.

The second peak hardness value observed in the base alloy is 110HV at outer zone. In contrast, the peak hardness values were observed in FG-composites with maxima towards the inner zone ranging from 120HV-155HV depending on increased volume fraction of Mg_2Si precipitates.

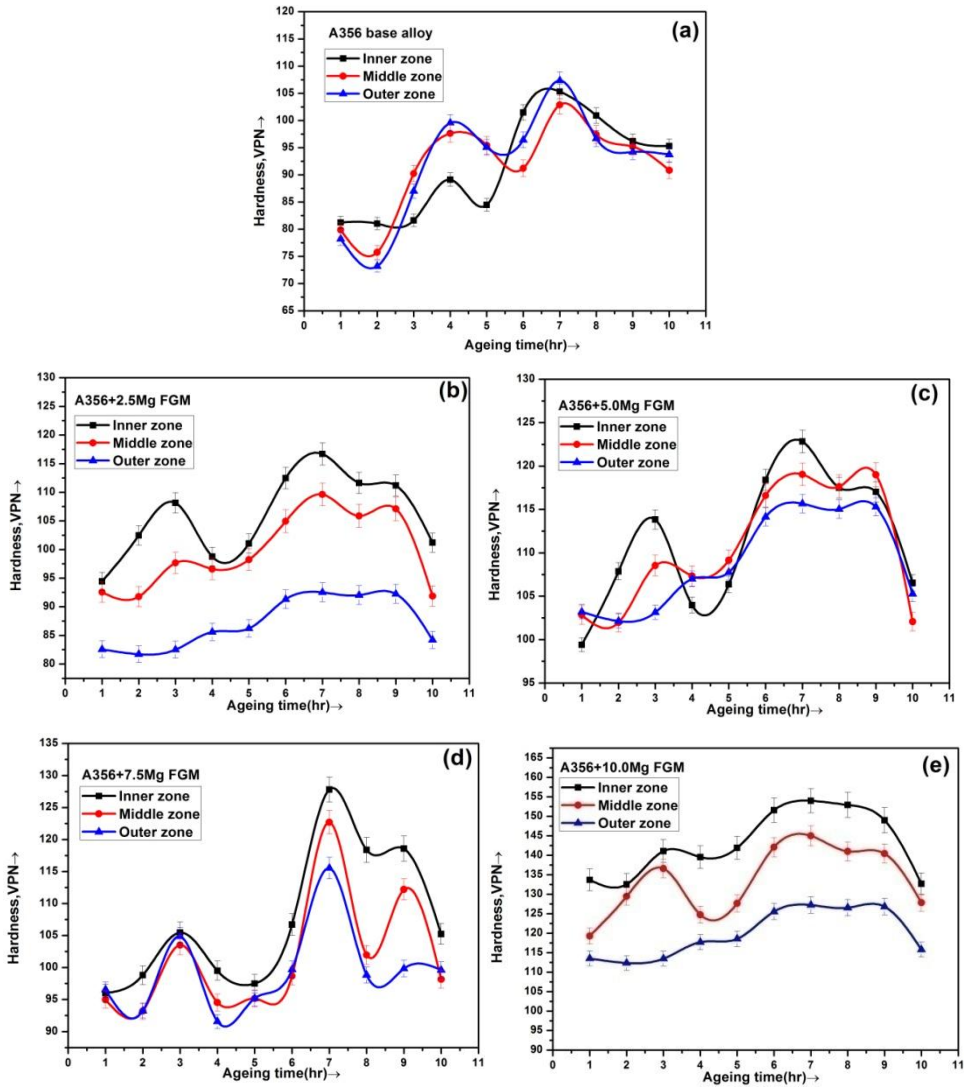

Fig.6.13 Vickers Hardness profiles for different zones of (a)A356 base alloy, (b)A356+2.5Mg,(c) A356+5.0Mg, (d)A356+7.5Mg & (e)A356+10.0 Mg FGMs in solution treated and aged conditions.

6.5.2 Ageing effect on tensile properties

Engineering stress-strain diagram of the solution treated and aged of base alloy and FG-composites with varying Mg content at different zones are shown in Figs.6.14-6.18. per ageing sequence described β' and Q'' are the phases present at second peak. The metastable β' and Q'' are responsible for strengthening the matrix at this state of ageing. These nano-sized particles semi-coherent with the Al matrix in combination with refined eutectic structure and primary Mg_2Si reinforcements are responsible for improved hardening response of the FG-composites [109,110]. The UTS are observed to be varying with Mg content in the composites.

For A356+10Mg FGM, the peak strength is about 263MPa. For the A356+7.5Mg FGM is 254.8Mpa, The tensile strength (UTS) of the A356+2.5Mg and A356+5.0Mg FG-composites is in the range of 160MPa and 290.48 MPa at the peak ageing condition. The slightly higher strength was observed in the A356+5Mg FGM at 150°C. The effect of test temperature on the strength and ductility has also been evaluated for the inner zone to the outer zone of the composites.

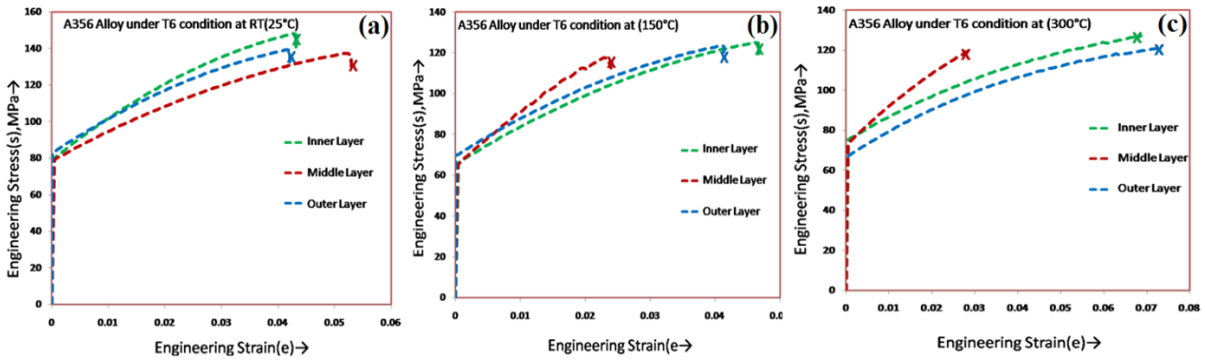

Fig. 6.14 Typical Engineering stress-strain diagrams for different zones of FG composites at; (a) RT (25°C), (b) 150°C and (c) 300°C of for base alloy after solution heat treated at 495 °C and aged at 160°C for 7h.

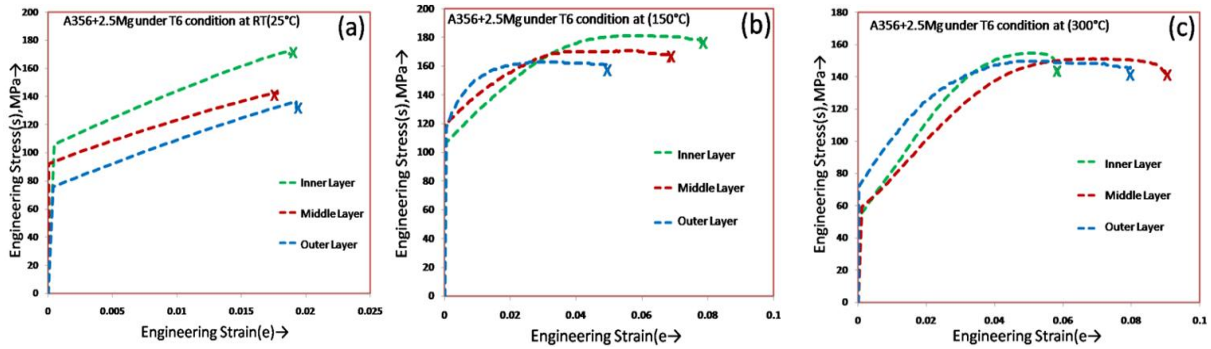

Fig. 6.15 Typical Engineering stress-strain diagrams for different zones of FG composites at; (a) RT (25°C), (b) 150°C and (c) 300°C of for A356-2.5%Mg FGM were solution heat treated at 495 °C and aged at 160°C for 7h.

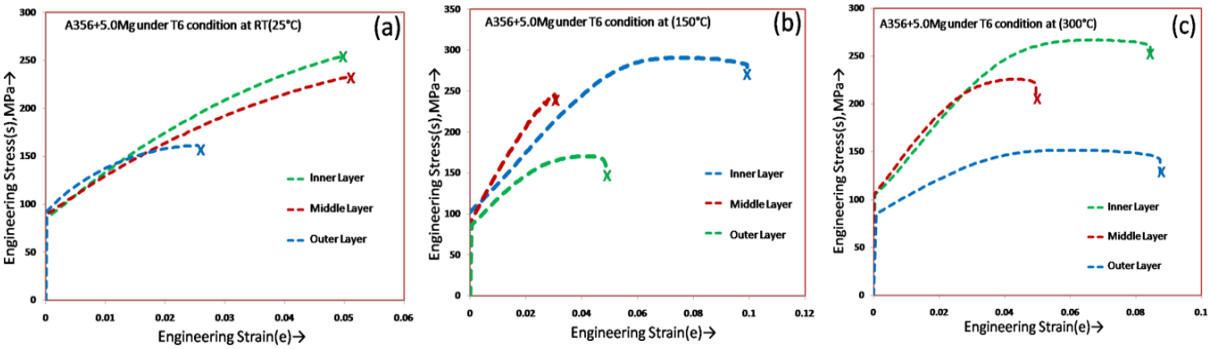

Fig. 6.16. Typical Engineering stress-strain diagrams for different zones of FG composites at; (a) RT (25°C), (b) 150°C and (c) 300°C of for A356-5%Mg FGM were solution heat treated at 495 °C and aged at 160°C for 7h.

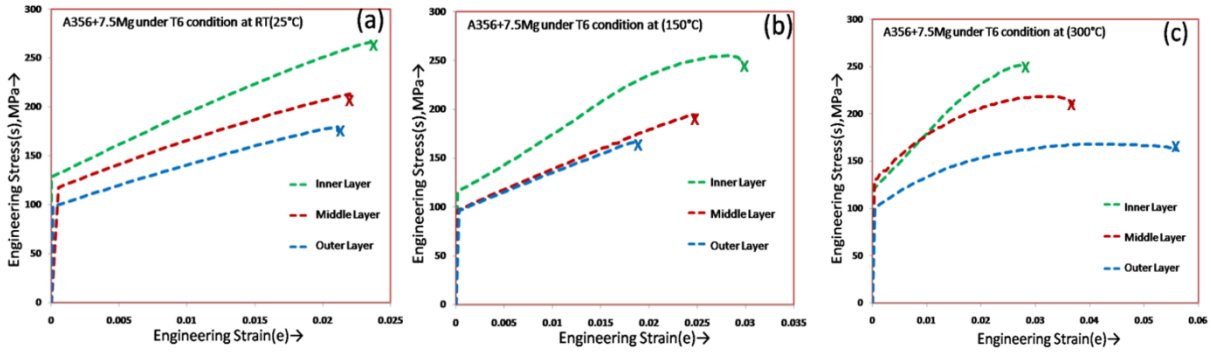

Fig. 6.17. Typical Engineering stress-strain diagrams for different zones of FG composites at; (a) RT (25°C), (b) 150°C and (c) 300°C of for A356-7.5%Mg FGM were solution heat treated at 495 °C and aged at 160°C for 7h.

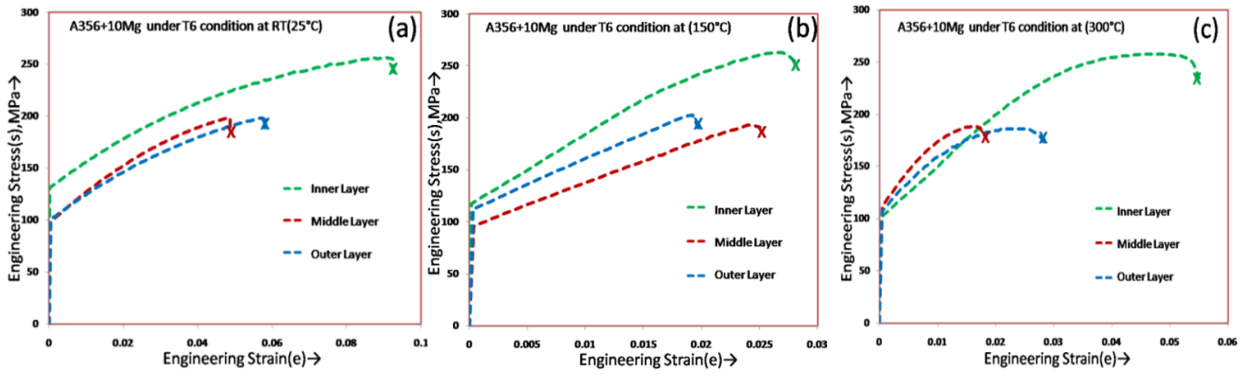

Fig.6.18. Typical Engineering stress-strain diagrams for different zones of FG composites at; (a) RT (25°C), (b) 150°C and (c) 300°C of for A356-10%Mg FGM were solution heat treated at 495 °C and aged at 160°C for 7h.

Fig.6.19 shows the UTS vs test temperature graphs after T6 heat treatment of cast composites. The plot shows the maximum UTS value at inner zone about 290.5MPa of A356+5Mg at 150°C test temperature. It can be also seen the tensile strength of the cast composites were enhanced after solutionization and ageing treatment. However as-cast Al–Mg_2Si FG-composites showed the lower UTS and elongation values, as illustrated in Chapter 5. The ultimate tensile strength (UTS) at room temperature also depicts maximum at the inner zone and increasing with Mg content. While the test temperature is raised to 150°C, A356-2.5%Mg FGM shows a maximum peak value of 178 MPa and a further increase in test temperature to 300°C causes softening. However, the UTS of A356-7.5%Mg is of lower UTS of 148 MPa was observed.

So far as the effect of varying wt.% Mg on the UTS of inner zones and to some extent middle zones are concerned, two opposite contributions viz. i) volume% of Mg_2Si reinforcements and ii) %porosity in the zone are to be considered. The strength is increasing as the volume% Mg_2Si is increased due to higher work hardening rate against plastic flow. On the contrary, porosity has a negative effect on the tensile strength and maximum porosities are observed at the inner zones and gradually decreasing towards

outer zones. Inner zones with 7.5% and 10% Mg should have better UTS than those of 2.5% and 5%Mg composites but the effect of porosity overshadows the effect of reinforcement volume% leading to a slight decrease in strengths. However, outer zones in all the FG-composites are having much lesser %porosities; the %Mg additions play a predominant role in increasing the strength as per the increasing percentage of eutectic Mg_2Si as well as nano-sized ageing precipitates.

It is important to note that the cast MMCs basically suffer from lack of ductility [110-111]. Very interesting results obtained from elongation values after homogenizing and ageing heat treatment, which are presented in Fig. 6.21 for all FG-composites. It is clear that in all specimens, including as-cast and heat treatment leads to an improvement in tensile ductility of the composite. The ductility improvement of the MMC by solutionizing treatment has been reported by Malekan et al. [112]. As Fig. 6.20 shows, the strain hardening exponents versus tensile test temperature for FG-composites after T6 heat treatment. This could be attributed to the reduction of strain hardening exponent (n) values with increases the teat temperature. The movement of dislocations increases causing annihilation and reduce their accumulation/pile up at grain boundaries.

The elongation value of FG-composites about 10% was achieved in the outer region after homogenized and aged samples. As discussed in chapter 5 as cast composites, the reductions of elongation were observed at inner zone due to presence of hard Mg_2Si particles. In contrast at the outer zone, the elongation values are increased due low volume fraction of particles. Sometimes, porosity content can also affect the elongation of

components.

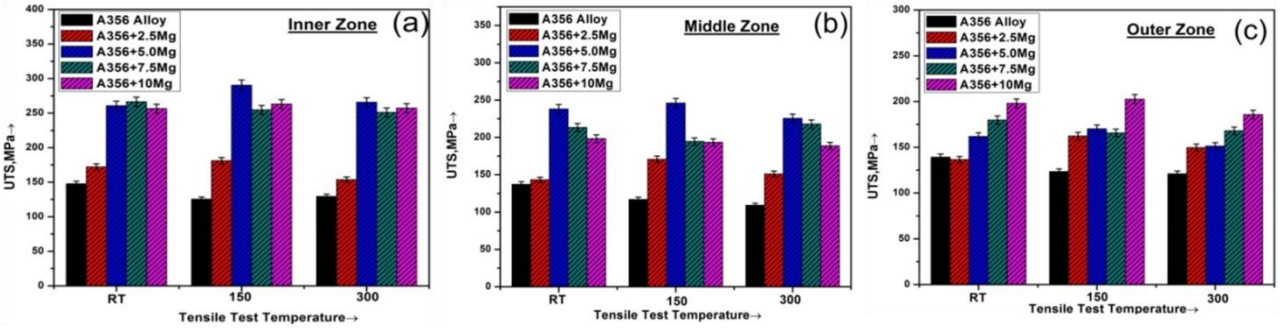

Fig.6.19 UTS(MPa) vs. test temperature graphs of FGMs after solution treated at 495°C for 7h and 10 h ageing time at 160°C in steps of 1h at (a)inner, (b)middle &(c) outer layers.

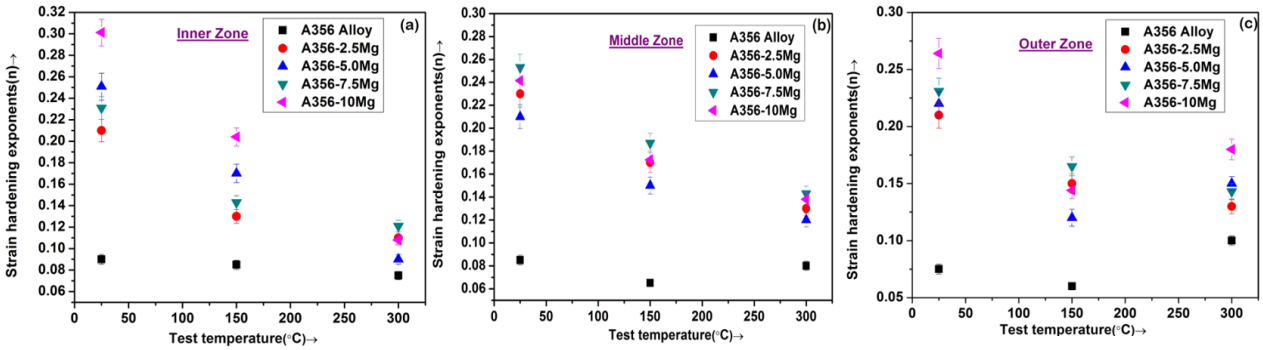

Fig.6.20 Strain hardening exponents vs. test temperature graphs of FGMs after solution treated at 495°C for 7h and 10 h ageing time at 160°C in steps of 1h at (a)inner, (b)middle &(c) outer layers.

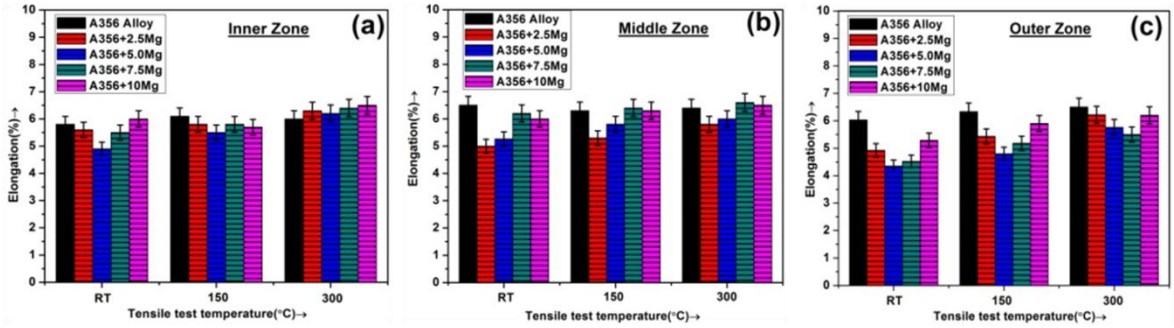

Fig.6.21. %Elongation graphs after solution treated at 495°C for 7h and 10 h ageing time at 160°C in steps of 1h;(a) A356+2.5Mg,A356+5.0Mg and(b) 7.5Mg, A356+10Mg FGMs at inner, middle& outer layers at different test temperature.

6.5.2.1. Strengthening Mechanisms

There are contributions of several probable strengthening mechanisms operative to the ultimate tensile properties of the FG-composites as follows:

i) Precipitation strengthening of the matrix

Orowan dislocation bypassing is the operative mechanism for GP zones, ß' and Q' metastable precipitates in T6 conditions coherent or semi-coherent with the matrix. However, for primary Mg_2Si particles Orowan strengthening is not effective because of their larger sizes. Orowan strengthening is appreciable if the sizes of the precipitates are below 1μm.

ii) Load –bearing strengthening

Direct strengthening results from load transfer from the matrix to the reinforcement via shear stresses at the interfaces. Since, the Mg_2Si particles are having high Young's modulus (120 GPa) and the particle/matrix interface bonding is good, the matrix is able to transfer the load to reinforcements Mg_2Si.

iii) Thermal mismatch strengthening

Increased density of dislocations are generated because of the differential thermal contraction between the matrix and the reinforcements during cooling from an elevated temperature of heat treatment. The Mg_2Si has a low co-efficient of thermal expansion ($7.5 \times 10^{-6} K^{-1}$) which is quite different from the matrix alloy ($22 \times 10^{-6} K^{-1}$). High dislocation densities are generated due to the difference in co-efficients of thermal expansions.

iv) Strengthening due to grain refinement

With refinement of grains the number of grain boundaries would increase which will hinder the dislocation motion and continuously accumulated at grain boundaries during deformation. However, as grain refinement with increasing Mg_2Si content is not appreciable the strength increase due to grain refinement is limited.

6.5.3. Characteristics of tensile fractures

The Fig.6.22 to 6.25 shows typical fracture surfaces of T6 heat treated in-situ FG-composites in different three different layers at RT, 150°C and 300°C. The features are more or less similar to those in the fractographs in as-cast conditions. However, the fracture nature is predominantly ductile with T6 treatment. The fracture modes are changing from mixed mode to ductile mode with increase in test temperature. The proportion of cleavage fracture is reduced considerably. Cracking of some eutectic Si are prominent in most of the fractographs. The inner zones of all samples show matrix/reinforcement interface debonding and nucleation of voids. This type of void nucleation is observed even at room temperature testing which could only be seen at high temperature fractures in case of as-cast composites. The fine fiber or spheroids of eutectic Si particles favor the localized shearing which leads to difficulty in crack initiation and propagation. Consequently, the tensile ductility after T6 treatments have been improved much compared to those in as-cast condition.

At lower test temperatures, the particle/ matrix interface is strong enough, and the stress can be transferred from the matrix to the reinforcing particles. With increasing test temperature, the strength of the particle/matrix interface decreases with simultaneous softening of the Al matrix. Thus, it is easier to accommodate the reinforcing particles.

Cracks are initiated at the matrix interface and propagate along the interface. Different modulus and thermal expansion of the reinforcing particles and the matrix and simultaneous softening of the Al-matrix are also supposed to be responsible for high temperature fracture characteristics.

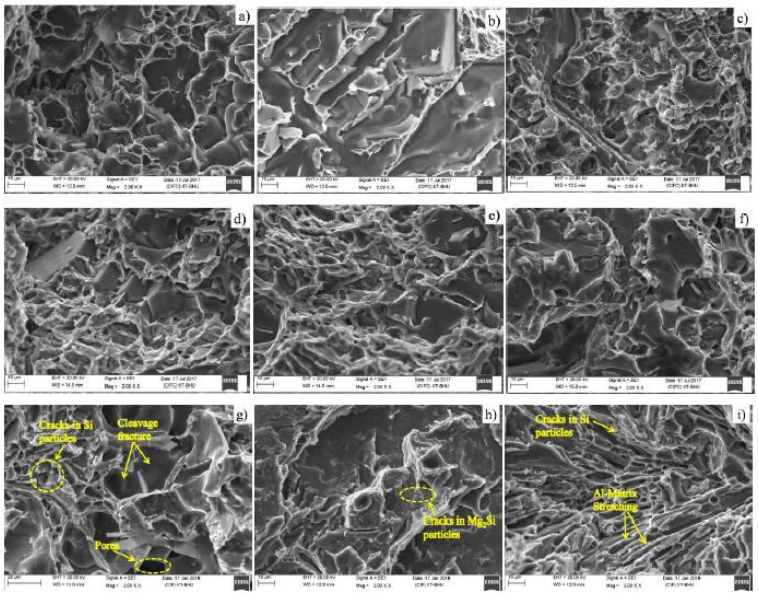

Fig.6.22. Typical Fractographs of A356+2.5Mg FGMs, a) inner zone, b) middle zone, and c) outer zone at 300°C respectively.

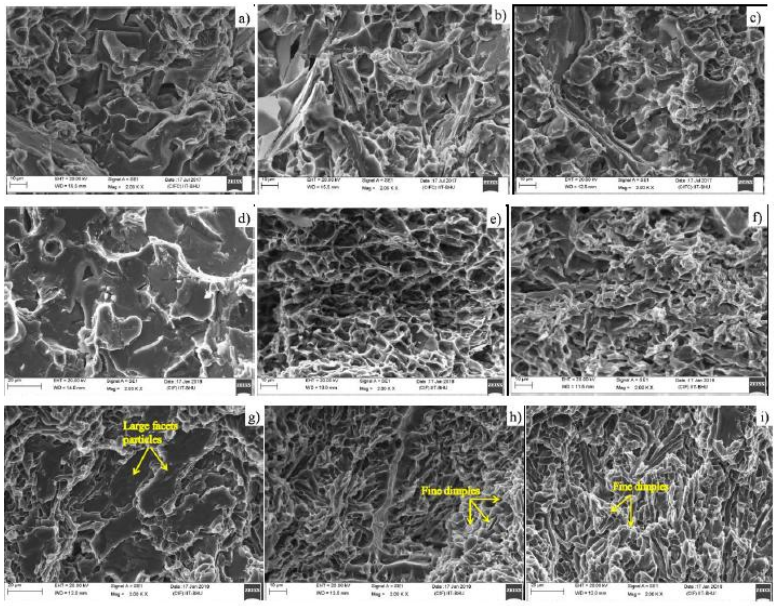

Fig.6.23. Typical Fractographs of A356+5.0Mg FGMs, a) inner zone, b) middle zone, and c) outer zone at 300°C respectively.

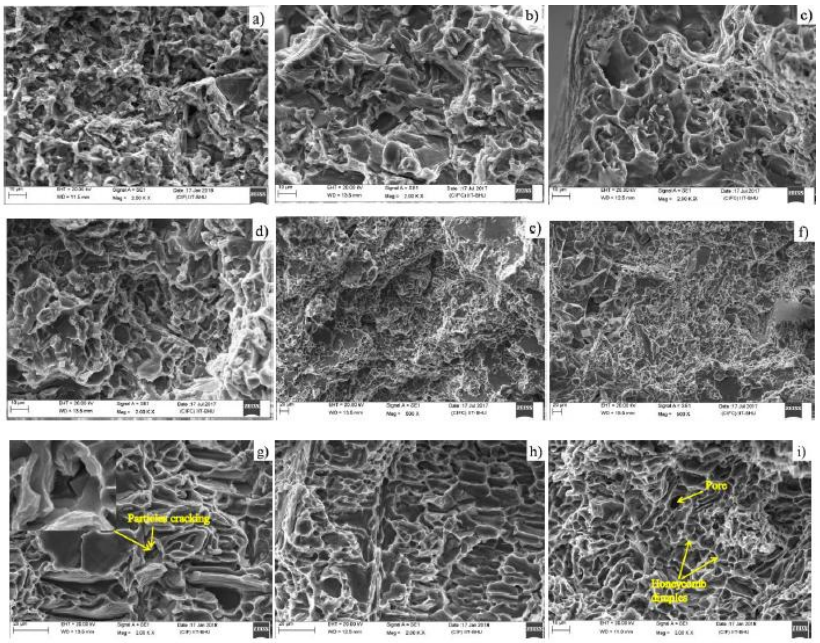

Fig.6.24. Typical Fractographs of A356+7.5Mg FGMs, a) inner zone, b) middle zone, and c) outer zone at 300°C respectively.

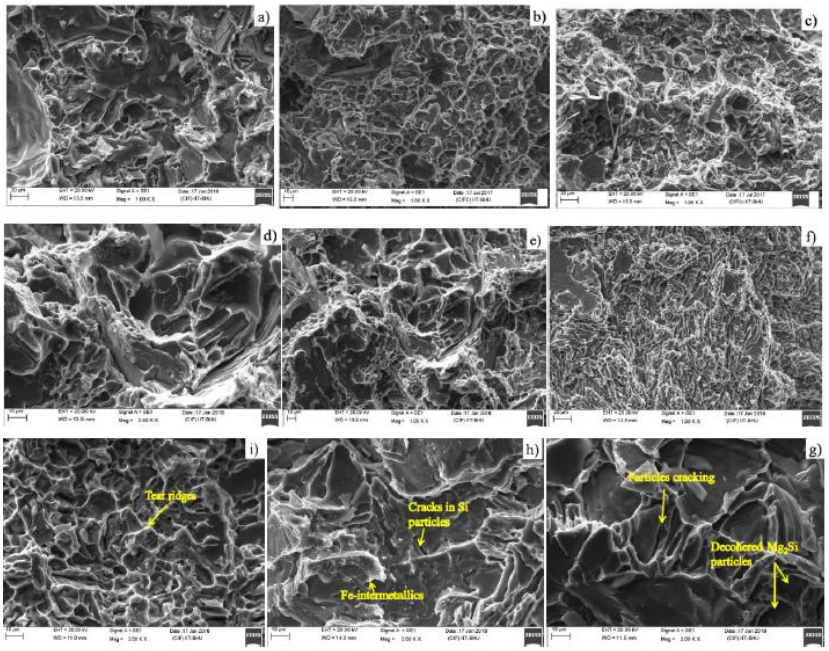

Fig.6.25. Typical Fractographs of A356+10Mg FGMs, a) inner zone, b) middle zone, and c) outer zone at 300°C respectively.

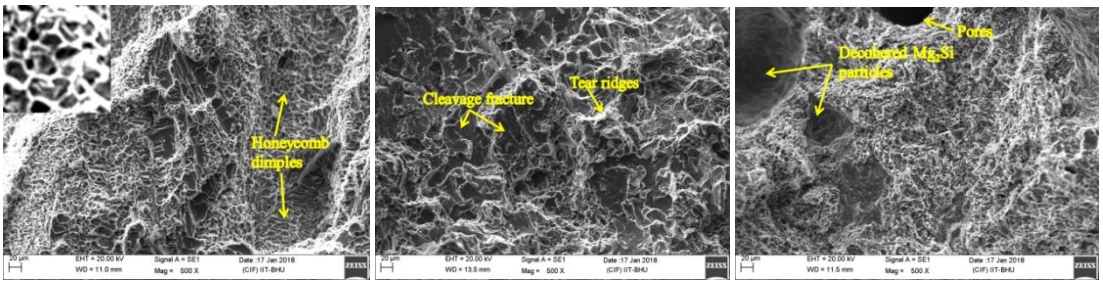

Fig.6.26 Typical Fractographs of FGMs, a)A356+5Mg (RT-25°C) outer zone, b) A356+7.5Mg at (150°C) middle zone, and c)A356+10Mg at inner zone at (300°C) respectively.

Fig.6.26 shows the typical fractured surfaces of tensile test samples at different test temperatures. From the Fig 6.26(a), the fracture surface at outer region of A356+5Mg FG-composites at room temperature shows a honey comb like structure due the presence of dense Al-Si eutectic phase and weak interface bonding. The tear ridges was observed in the middle layer of FG-composites refer to Fig.6.26 (b) showing the softness and reduction of composites strength. Some of the voids and decohesion of particle was also observed as shown in the Fig.6.26(c) indicating the reduction of strength of the FG-composites.

6.6. Chapter summary

- The eutectic Si showing a remarkable change from coarse acicular to spheroidized refined particles in base alloy A356 upon solution treatment and ageing. This is due to fragmentation or dissolution of eutectic Si branches and subsequent spheroidization of separated branches.
- In FG-composites the eutectic Mg_2Si particles are also more or less spheroidized. The primary Mg_2Si particles undergo a considerable shape change however the sizes are remaining almost same. Sharp corners are rounded up during solution treatment as a result of diffusion of Si and Mg from preferential sites. Flaky Fe-intermetallics are reduced but some blocky $CuAl_2$ intermetallics and 'Q' phase are

still remaining. These are formed during solidification and are not dissolved totally during solution treatment.

- Freshly formed nano-sized β" and β' –Mg_2Si are formed during ageing from clusters of GP zones which strengthens the matrix by precipitation strengthening. The microstructures correspond to second highest peaks in the ageing curves. Along with β', Q'' phase is also probable, but this could be revealed only by HRTEM.
- The ageing curves (hardness vs. ageing time) show triple peak phenomenon- three hardness peaks are observed with the progress of ageing. This conforms the precipitation sequence. The first peak arises due to the formation of metastable β" phase and subsequently the β' phase formation gives rise to second peak. The actual precipitated phase giving rise to third peak could not be examined. However, from earlier research reports these can be attributed to the precipitation of Q', θ', β' and some Si.
- Remarkable increases in tensile strengths are observed after solution treatment and ageing as compared to those in as-cast conditions. As expected, inner zones develop maximum strength due to segregation of primary Mg_2Si particles in combination with fine semi-coherent β' and/ or Q'' precipitates formed during ageing.
- The improved tensile strength observed in the FG-composites is due to combined strengthening mechanisms of matrix strengthening due to precipitation strengthening, load-bearing strengthening by the reinforcements and strengthening due to thermal mismatch of reinforcements and the matrix.